Rock Mech. Rock Engng. (2001) 34 (2), 135–159

**Rock Mechanics and Rock Engineering**


# Finite Element Analysis of a Deep-seated Slope Deformation

**F. Forlati**[1], **G. Gioda**[2], and **C. Scavia**[3]

[1] Geological Service of Piemonte Region, Turin, Italy
[2] Department of Structural Engineering, Politecnico di Milano, Milan, Italy
[3] Department of Structural and Geotechnical Engineering, Politecnico di Torino, Turin, Italy

## Summary

A study is presented of the slow time dependent movement of the deep-seated deformation of Rosone. This rock slope, which mainly consists of gneiss, is located on the Italian side of Western Alps and has been affected by recurrent instability phenomena. Due to these, and also to the presence of various villages and man-made structures (such as a hydroelectric power plant), a significant amount of geological and geomechanical data has been collected in this area. They have led to the assumption that the slow movement develops along a deep-seated sliding surface, involving a volume of rock between 22 and 35 million cubic meters. To check these hypotheses, and to get some insight into the causes of the phenomenon, a series of non-linear, time-dependent analyses has been carried out through the finite element method. The slow movement of the rock mass, and the gradual loss of its mechanical properties with increasing deformation, has been accounted for in the calculations by means of a visco-plastic constitutive law, allowing for strain softening effects. The results of analyses lead to some conclusions on the causes of the observed movements, among which the possible influence of the groundwater pore pressure is likely to play an important role.

## 1. Introduction

A widespread presence of deep-seated slope deformations ranging in size from some tenth to several $km^2$ has been identified in the valleys of the Western Alps (see e.g. Mortara and Sorzana, 1984; Forlati et al., 1995). It has also been recognised that these slope deformations can evolve into large landslides, under conditions that may be present in many of the identified cases (Forlati and Mortara, 1994).

The evaluation of the risk engendered by instability phenomena is essential for civil protection actions aimed at preventing, or minimising, the consequent damages. To this purpose, it is necessary to identify the possible failure mechanisms and to choose proper methods of analysis for assessing the degree of stability of the slopes.

With reference to the numerical modelling of large gravitational deformations of slopes, it is recognised that some additional problems are involved with respect

**Fig. 1.** Location of the investigated area (black square dot) in northern Italy

to those encountered in the analysis of smaller landslides. They are mainly related to the difficulties met in defining the geometry and boundary conditions of the moving mass, the causes of the movements underway, and the overall mechanical characteristics of the rock mass.

For such reasons the numerical analysis of these phenomena has to be supplemented by other studies (e.g., geological, geomorphological, geomechanical) in order to validate its basic assumptions and to verify the results of calculations.

Here a geomechanical and numerical study is discussed that concerns the deep-seated deformation of Rosone, located on the Italian side of Western Alps (Fig. 1).

Owing to the presence of significant elements of risk in the area (several villages, a hydroelectric power plant and a highway), the Rosone slide has been thoroughly investigated by the Geological Service of the Piemonte Region. This led to a large collection of geological and geomechanical studies (e.g. Forlati et al., 1991), and to numerical investigations (e.g. Barla and Chiriotti, 1995; Chiriotti, 1997) on the overall behaviour of the slide.

In the following, the main characteristics of the slide are first outlined and a summary is presented of the geomechanical investigation carried out in the recent years. Subsequently, the numerical part of the study is discussed that concerns, in particular, the modelling of the evolution of the "mechanical damage" within the

moving mass and the identification of the possible causes of the displacements recorded in the field.

The analyses were performed with reference to a continuum equivalent model of the rock mass, and by adopting mechanical parameters scaled down with respect to those of the rock material.

The main features of the adopted finite element model are described, considering the choice of a proper constitutive law for the overall rock mass and the calibration of its parameters. On the basis of the numerical results, some conclusions are drawn concerning the possible causes of the phenomenon and the potential use of numerical models in the analysis of this kind of large-scale instability problems.

*Notation*: Upper and lower case underlined letters denote, respectively, matrices and column vectors. The superscript T means transpose and a superposed dot means time derivative.

## 2. Historical and Geological Background of Rosone Landslide

The entire southern side of the ridge bounded by the Orco and Piantonetto rivers, in the Province of Turin, has been undergoing a slow process of deep-seated gravitational deformation. This phenomenon, which involves an area of about 55 km$^2$ and reaches a depth of over 100 m (Ramasco et al., 1989), affects a 1300 m high slope, from an altitude of 2000 m at the ridge crest down to 700 m at the valley bottom (Fig. 2).

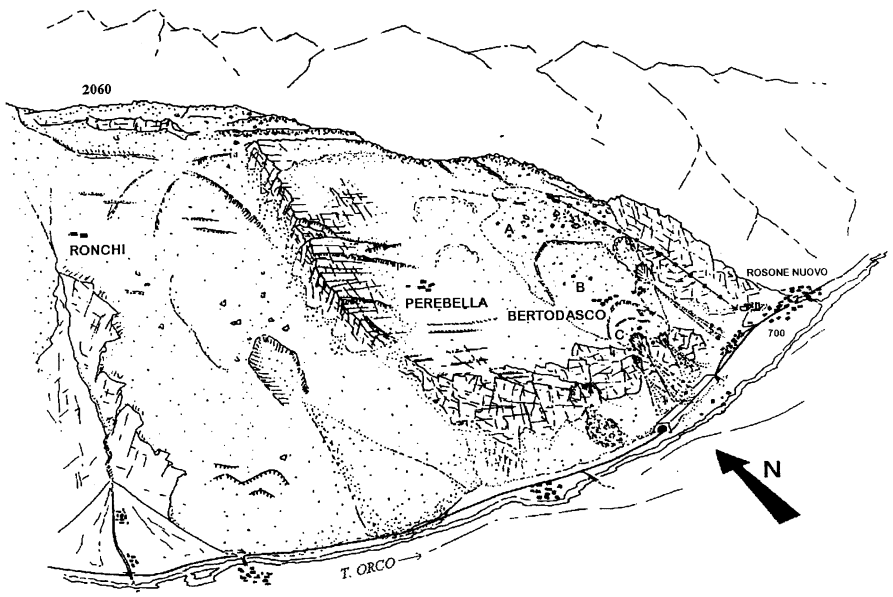


**Fig. 2.** Schematic representation of Rosone slope (after Forlati et al., 1991)

Because of this deformation process, a vast landslide movement, historically known as Rosone landslide, developed near the villages of Rosone and Bertodasco. Due to the consequent damages produced in the old settlements, a new village was built up in 1956. This new village (named Rosone Nuovo) is close to the merging of the two mentioned streams and to a 99 MW hydroelectric power plant of the AEM (Electricity Agency of the city of Turin).

Two major stages of paroxysmal movement have been recorded: one in the early 18th century and another in the fall-winter of 1953. Presently, significant movements are still taking place in the upper part of the landslide zone.

The Orco valley, where the Rosone landslide is located, belongs to the central part of the Gran Paradiso massif. The geological configuration of the area is relatively simple: mostly outcrops of granite and gneiss. Levels of mica schist, as well as of chlorite schist, are also present.

A comparative analysis of glacial geomorphology and subsequent fluvial erosion shows that the southern side of the Orco-Piantonetto ridge, corresponding to a vast mass movement developed near Bertodasco, represents a transfluence zone generated by the lateral Piantonetto glacier constriction. A schematic plano-altimetric ice distribution during the Quaternary glacial period, derived from geomorphological analyses based on the interpretation of aerial photographs, made it possible to identify the altitude of 1560 m as the maximum level reached by the ice in the area under examination.

The annual rainfall was observed over a period of 42 years, from 1938 to 1980. Its average value, of about 1200 mm, corresponds to a station located in the centre of Rosone area, near the toe of the sliding slope, at an elevation of about 700 m.

The months of May and October are characterised by the highest monthly rainfall value (160 mm) and by the largest number (12) of rainy days. During the late spring days the snow cover melts away quickly. As a result, a considerable quantity of water seeps down into the sliding body. The flow of water in the slope occurs through the main discontinuities, which are generally open and persistent. Considering that the upper part of the slope acts as a reservoir, the largest part of the groundwater is cumulated when rainfalls combine with the melting of the snow cover. It should be also mentioned that perennial springs are present at Bertodasco and Perebella.

The morphological and structural characteristics of the area suggest subdividing it into three adjacent sectors, roughly corresponding to the villages of Perebella, Bertodasco and Ronchi (cf. Figs. 2 and 3). These sectors reflect, respectively, the early, intermediate and final stages of the evolution of a site subjected to a deep-seated gravitational process. On account of the presence of such widely diversified conditions in a single area, this site turns out to be particularly suited for stability studies and to their comparative evaluation (Forlati et al., 1991).

Examining the area from west to east, the Ronchi sector is met first, characterised by a highly advanced stage of evolution of the deformation that has caused the disruption of the original rock formations. This sector may now be deemed to be substantially stable.

The central sector, around Perebella, reflects an early stage in the deformation process. It is clearly separated from the Ronchi sector by a scarp running in the

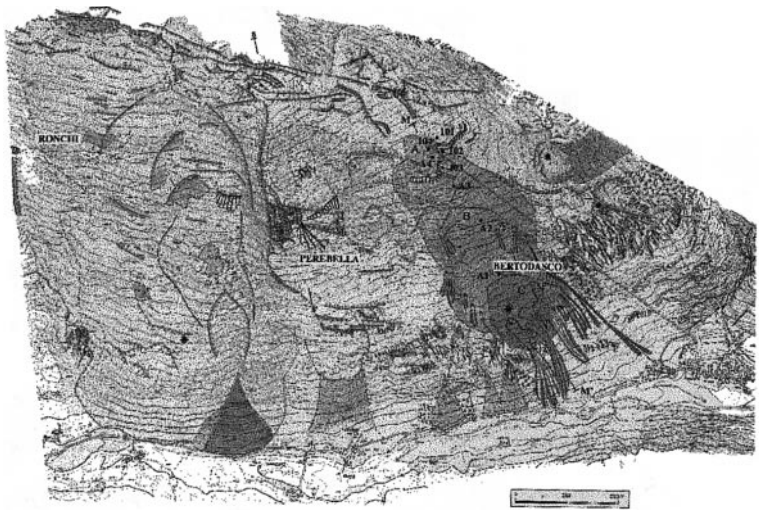


**Fig. 3.** Morpho-structural elements of Rosone slope and its main scarps and trenches. The shades from light to dark indicate increasing stages of the slope instability process (after Forlati et al., 1991)

NS direction and developing over a few hundred meters. This presents the formation of a major lateral scarp that separates the two areas with differences in level of up to 50–90 m. The large outcrops of the rock substratum in this area appear fractured in their middle and lower portions.

As to the eastern sector of Bertodasco, which is inhabited and hosts the AEM electric power plant, the historical data make it possible to classify its current stage of deformation as intermediate between those of Ronchi and Perebella sectors.

Previous studies (Forlati et al., 1991) made it possible to identify the Bertodasco sector as the one most likely to undergo a catastrophic evolution. The interpretation of aerial photographs revealed also the presence of three areas with different degrees of mobility, from the top to the floor of the valley, referred to as A, B and C in Fig. 2.

## 3. Geomechanical Studies

The geomechanical studies of the Bertodasco sector, carried out in the recent years, can be summarised as follows:

a) Surface investigations for the characterisation of the rock mass and of its discontinuity systems. Three main systems have been identified (Fig. 4), namely: the schistosity, $S_S$ (dip direction of 154°, dip of 34°), and two main joint sets, $S_1$ (dip direction of 203°, dip of 86°; dip direction of 15°, dip of 68°) and $S_2$ (dip direction of 277°, dip of 80°; dip direction of 100°, dip of 85°).
b) Deep investigations, consisting of the drilling of boreholes, with continuous coring, up to a depth of 120 m. Particular attention was given to boreholes A1–A4, on account of their location along the maximum inclination line (Fig. 5).

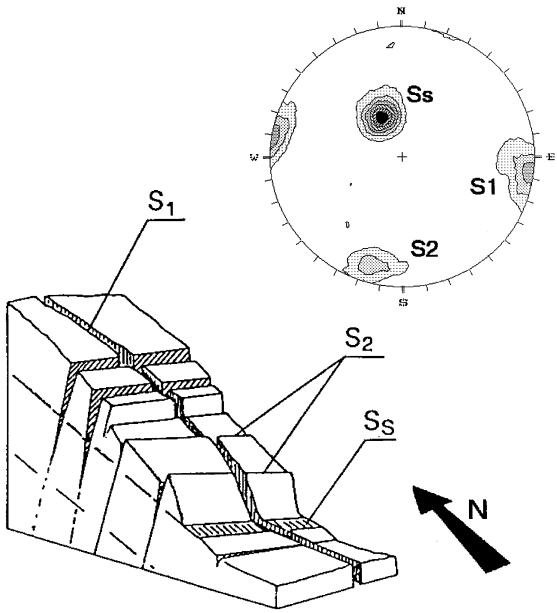


**Fig. 4.** Schematic block diagram and stereographic projection of the principal joint sets ($S_1, S_2$) and of the schistosity plane ($S_S$)

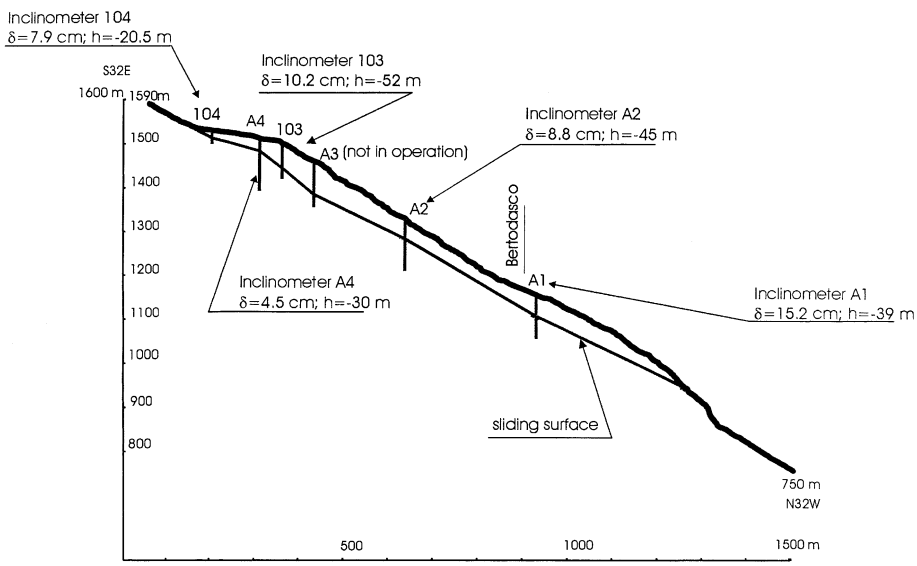


**Fig. 5.** Cross section of Rosone landslide and location of the inclinometers. The shape of the sliding surface has been derived from the inclinometer measurements; $h$ represents the depth of the sliding surface; $\delta$ denotes the maximum horizontal displacement recorded between December 1984 and August 1998, for inclinometers 103 and 104, and between December 1991 and August 1998, for inclinometers A1 to A4

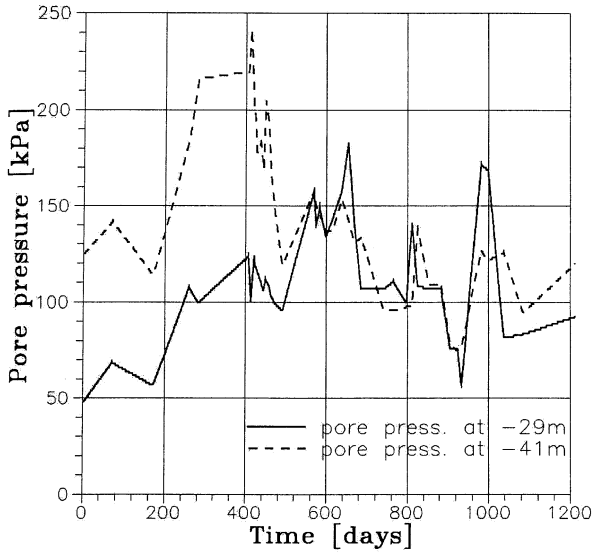


**Fig. 6.** Pore pressure vs. time measurements from piezometer A1 (cf. Fig. 5) at 29 m and 41 m depth

c) Laboratory tests performed on intact and fractured samples of the rock recovered from the borings. These tests provided the following average values of the relevant mechanical parameters for the rock material: unit weight of 26.5 kN/m$^3$ and uniaxial compression strength $C_0$ of 110 MPa. The schistosity is characterised by a friction angle of 34°, a Joint Roughness Coefficient JRC of 11, and a Joint Compressive Strength JCS of 75 MPa.

Two piezometers have been installed at two different depths (29 m and 41 m) in borehole A1. Figure 6 shows the variation during time of the piezometric level, recorded from June 1992 to April 1996. The interpretation of these data is not straightforward, due to the complex hydrogeological conditions of the slope. In addition, no reliable correlation has been established so far between the evolution of the hydraulic pressure during time and the amount of rainfall.

The boreholes were instrumented with inclinometers. The recorded data confirm the existence of 3 zones with different degree of mobility (from 1 cm/year in zone A to 2.4 cm/year in zone C). These data show also the presence of a clear discontinuity in the displacements. This suggests the existence of a deep-seated failure surface inside the slope that should lead to a volume of the moving rock mass between 22 and 35 million cubic meters. Figure 5 presents a section of the slide and of the assumed failure surface, and the location where the inclinometers have been installed.

The described geomechanical model represents the basis of the numerical study described in the following Sections. This part of the study intends to get some insight into the overall mechanical behaviour of the rock mass, and to assess the influence of the glacier action. In addition, an attempt is made to verify the hypothesis of a deep-seated failure surface and to investigate the possible correlation

between the variation of the pore pressure during time and the displacements recorded in the field.

## 4. Visco-plastic Constitutive Law

The slow downward movement of the landslide could be accounted for in a numerical calculation through a proper constitutive "creep" law for the rock mass. The time dependent behaviour of rocks has been extensively studied in the literature from both experimental and theoretical points of view (Cristescu, 1988; Ladanyi, 1993; Cristescu and Gioda, 1994), leading to a variety of analytical (see e.g. Fritz, 1984) and numerical solutions based, in particular, on the finite element method. These have been mainly applied to tunnels and underground openings and range from the use of relatively simple visco-elastic models to that of more complex visco-plastic laws (see e.g. Zienkiewicz and Pande, 1977; Ghaboussi and Gioda, 1977; Gioda, 1981; Kovari and Fritz, 1983). However, some notable applications to slope stability problems have been also presented in the literature (Vulliet, 1995, 2000), which involve new developments related, in particular, to the use of a Neural Network approach.

The elasto-visco-plastic model adopted for the purposes of this study (depicted in Fig. 7 for the one-dimensional case) can take into account the so-called secondary and tertiary stages of the creep behaviour of the rock mass.

Under low stress levels, not exceeding the yield limit of the frictional slider, the model exhibits a reversible "instantaneous" behaviour governed by the Hook element (spring). If the applied stress (constant with time) overcomes this limit, its exceeding part is carried by the viscous element (dashpot). Hence, secondary creep shows up that corresponds to a constant rate of deformation if the mechanical parameters of the dashpot do not vary with the stress/strain state. Tertiary creep, characterised by a strain rate increasing with time, can be introduced by providing suitable laws relating the decrease of the shear strength, and viscosity, parameters to the cumulated creep strains.

Visco-elastic, or primary, creep was not introduced into the calculations considering that this reversible time dependent effect has a minor influence on the overall behaviour of the slope.

Note that the adopted elasto-visco-plastic model reduces to a standard elasto-plastic model if its viscosity is neglected in the calculations. However, the numerical solution technique described in the next Section has been specifically developed for visco-plastic analyses and it would not be adequate for applications to the elasto-plastic case.

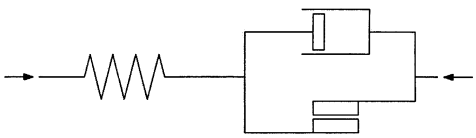

**Fig. 7.** Elasto-visco-plastic rheological model

To describe the governing equations of the creep model, let us consider first the case in which the material parameters are constant during the deformation process. A main hypothesis adopted in the following is that the material is isotropic and that the viscous element carries only deviatoric stresses while, as customary, the frictional element is subjected to both volumetric and deviatoric stresses, depending on its constitutive relationship.

Consider the stress state at time $t$, represented by vector $\underline{\sigma}_t$, and assume that a part of it $\underline{\sigma}_t^y$ acts on the frictional element, while its remaining part $\underline{\sigma}_t^{cr}$ acts on the viscous element,

$$\underline{\sigma}_t = \underline{\sigma}_t^y + \underline{\sigma}_t^{cr}. \tag{1}$$

The stress vector $\underline{\sigma}_t$ can be subdivided into its volumetric $(\sigma_{\text{vol}})_t$ and deviatoric $\underline{s}_t$ components. As previously mentioned, the volumetric component acts on the frictional element, while the deviatoric part can be further subdivided into its components carried by the frictional element $\underline{s}_t^y$ and by the dashpot $\underline{s}_t^{cr}$,

$$\underline{\sigma}_t^y = \underline{m} \cdot (\sigma_{\text{vol}})_t + \underline{s}_t^y, \quad \underline{\sigma}_t^{cr} = \underline{s}_t^{cr}. \tag{2a,b}$$

In the above equation, $\underline{m}$ is a vector the entries of which are equal to 1, if they correspond to normal stresses, or to 0, if they correspond to tangential stresses,

$$\underline{m}^T = \{111000\}. \tag{3}$$

The stresses vector $\underline{\sigma}_t^y$ can be readily evaluated on the basis of the yield criterion of the frictional element, which is here defined by the Drucker-Prager condition,

$$F = J_2^{1/2} - \alpha I_1 - k = 0. \tag{4}$$

In Eq. (4), $J_2$ is the second invariant of the deviatoric stresses, $I_1$ is the first stress invariant and $\alpha$ and $k$ are shear strength parameters related to cohesion and friction angle.

The use of this yield condition, instead of other criteria such as Mohr-Coulomb or Hoek-Brown, depends on its simple form which permits the analytical evaluation of its gradient and a "robust" implementation into the finite element code. This aspect should not be overlooked when developing a relatively complex computer program for applications to actual engineering problems. In fact, it was decided to limit the complexity of the various "components" of the finite element model, to avoid further numerical problems when dealing with the analysis of the actual slide

The visco-plastic strain rate $\dot{\underline{\varepsilon}}_t^{cr}$ is subdivided into its volumetric $(\dot{\varepsilon}_{\text{vol}}^{cr})_t$ and deviatoric $\dot{\underline{e}}_t^{cr}$ parts,

$$\dot{\underline{\varepsilon}}_t^{cr} = \tfrac{1}{3}\underline{m} \cdot (\dot{\varepsilon}_{\text{vol}}^{cr})_t + \dot{\underline{e}}_t^{cr}, \quad \underline{m}^T \cdot \dot{\underline{e}}_t^{cr} = 0. \tag{5a,b}$$

Since the viscous and frictional elements are subjected to the same deformation, plastic and creep strains coincide. Consequently, the plastic flow rule can be expressed in terms of the creep strain rate $\dot{\underline{\varepsilon}}_t^{cr}$ through the following equation,

$$\dot{\underline{\varepsilon}}_t^{cr} = \dot{\lambda}_t \underline{n}_t, \tag{6}$$

where $\dot{\lambda}_t$ is the plastic multiplier and $\underline{n}_t$ is the gradient of the plastic potential $\Psi$ evaluated at $\underline{\sigma}_t^y$,

$$\underline{n}_t = \frac{\partial \Psi}{\partial \underline{\sigma}_t^y}. \tag{7}$$

The expression of $\Psi$ coincides with that of the yield function $F$ (Eq. 4). In this case a reduced value of the frictional parameter is adopted, to properly model the dilatancy effects, while it is not necessary to define the cohesive component of the plastic potential function, since the derivative in Eq. (7) rules it out.

Combination of Eqs. (6) and (5) leads to the following expression of the plastic multiplier,

$$\dot{\lambda}_t = \frac{(\underline{\dot{e}}_t^{cr})^T \cdot \underline{\dot{e}}_t^{cr}}{(\underline{\dot{e}}_t^{cr})^T \cdot \underline{n}_t}, \tag{8}$$

where vector $\underline{n}_t$ is given by Eq. (7) and the deviatoric creep strain rate $\underline{\dot{e}}_t^{cr}$ can be related to the deviatoric stress vector $\underline{s}_t^{cr}$ through the viscosity matrix $\underline{V}^{cr}$ of the dashpot,

$$\underline{s}_t^{cr} = \underline{V}^{cr} \cdot \underline{\dot{e}}_t^{cr}. \tag{9}$$

Note that, owing to the previous assumptions of isotropic and of purely deviatoric behaviour of the dashpot, $\underline{V}^{cr}$ is a diagonal matrix that depends only on one deviatoric viscosity coefficient $\eta$.

## 5. Time Integration Procedure

Upon discretization into finite elements, the governing equation of the time dependent problem can be written in the following general form, representing the equilibrium condition at time $t$ between the total applied forces $\underline{f}_t$ and those equivalent, in the finite element sense, to the total stresses $\underline{\sigma}_t$,

$$\sum \int_V \underline{B}^T \underline{\sigma}_t \, dv = \underline{f}_t. \tag{10}$$

Here, the summation runs over the elements of the mesh, $V$ represents the element volume and $\underline{B}$ is the matrix collecting the spatial derivatives of the displacement shape functions.

A convenient procedures for the numerical solution of time dependent problems is represented by the so called "initial strain" method (Zienkiewicz and Cormeau, 1974) according to which the stress vector at any time $t$ is expressed as,

$$\underline{\sigma}_t = \underline{D} \cdot [\underline{\varepsilon}_t - \underline{\varepsilon}_t^{cr}], \tag{11}$$

where $\underline{D}$ is the constitutive elastic matrix, governing the instantaneous response of the visco-plastic material, and $\underline{\varepsilon}_t$ and $\underline{\varepsilon}_t^{cr}$ are the vectors collecting, respectively, total and creep strains.

A simple iterative scheme for time integration can be based on the assumption of a constant creep strain rate during a time increment $\Delta t$. This leads to the fol-

lowing approximation of the creep strain increment for the $i$-th iteration

$$(\Delta\underline{\varepsilon}_t^{cr})^i = (\underline{\varepsilon}_t^{cr})^i - \underline{\varepsilon}_{t-\Delta t}^{cr} = \Delta t \cdot [\vartheta \cdot (\dot{\underline{\varepsilon}}_t^{cr})^{i-1} + (1-\vartheta) \cdot \dot{\underline{\varepsilon}}_{t-\Delta t}^{cr}]. \tag{12}$$

Here $\vartheta$ is a coefficient the value of which varies between 0 and 1. If $\vartheta = 0$, the creep strain increment depends only on the relevant quantities evaluated at the end of the preceding time increment, thus leading to an explicit integration scheme. However this scheme is in general affected by convergence and stability problems. To avoid this drawback, an implicit scheme is here adopted, with $\vartheta = 0.5$, which requires to performing the following calculations for the $i$-th iteration:

1) The nodal displacement increment $\Delta\underline{u}_t^i$ is computed at the beginning of the $i$-th iteration through a linear elastic analysis, on the basis of the stiffness matrix $\underline{\underline{K}}$ and of the unbalanced nodal force vector $\underline{r}_t^{i-1}$ evaluated at the end of the previous iteration,

$$\underline{\underline{K}} \cdot \Delta\underline{u}_t^i = \underline{r}_t^{i-1}. \tag{13}$$

The displacement and total strain vectors are then updated,

$$\underline{u}_t^i = \underline{u}_t^{i-1} + \Delta\underline{u}_t^i, \quad \underline{\varepsilon}_t^i = \underline{\varepsilon}_t^{i-1} + \Delta\underline{\varepsilon}_t^i. \tag{14a,b}$$

For the first iteration, the creep strain rate $(\dot{\underline{\varepsilon}}_t^{cr})^{i-1} = (\dot{\underline{\varepsilon}}_t^{cr})^0$ is assumed equal to that determined at the end of the preceding time increment, $\dot{\underline{\varepsilon}}_{t-\Delta t}^{cr}$, thus leading to the following form of Eq. (12), regardless the value assumed for $\vartheta$,

$$(\Delta\underline{\varepsilon}_t^{cr})^1 = \Delta t \cdot \dot{\underline{\varepsilon}}_{t-\Delta t}^{cr}. \tag{15}$$

The corresponding unbalanced force vector is then evaluated through the following relationship,

$$\underline{r}_t^0 = \Delta\underline{f}_t + \int_V \underline{\underline{B}}^T \underline{\underline{D}} \cdot (\Delta\underline{\varepsilon}_t^{cr})^1 \, dV, \tag{16}$$

where $\Delta\underline{f}_t$ is the increment of external loads for the current time step.

2) The stress increment for the current iteration is calculated on the basis of the total and creep strain increments and of the elastic constitutive matrix $\underline{\underline{D}}$, and the stress state is updated,

$$\Delta\underline{\sigma}_t^i = \underline{\underline{D}} \cdot [\Delta\underline{\varepsilon}_t^i - (\Delta\underline{\varepsilon}_t^{cr})^i], \quad \underline{\sigma}_t^i = \underline{\sigma}_t^{i-1} + \Delta\underline{\sigma}_t^i. \tag{17a,b}$$

3) A more accurate value of the creep strains at time $t$ is evaluated for the current iteration $(\underline{\varepsilon}_t^{cr})^i$ by means of the visco-plastic relationships and of Eq. (12), with $\vartheta = 0.5$, re-written for the relevant quantities,

$$(\underline{\varepsilon}_t^{cr})^i = \underline{\varepsilon}_{t-\Delta t}^{cr} + \tfrac{1}{2} \cdot [\lambda_t^i - \lambda_{t-\Delta t}] \cdot [\underline{n}_t^i + \underline{n}_{t-\Delta t}], \tag{18}$$

where

$$\lambda_t^i = \lambda_{t-\Delta t} + 2 \cdot \frac{[(\underline{e}_t^{cr})^i - \underline{e}_{t-\Delta t}^{cr}]^T \cdot [(\underline{e}_t^{cr})^i - \underline{e}_{t-\Delta t}^{cr}]}{[(\underline{e}_t^{cr})^i - \underline{e}_{t-\Delta t}^{cr}]^T \cdot [\underline{n}_t^i + \underline{n}_{t-\Delta t}]}, \quad \underline{n}_t^i = \frac{\partial \Psi}{\partial (\underline{\sigma}_t^y)^i}, \tag{19a,b}$$

$$(\underline{e}_t^{cr})^i = \underline{e}_{t-\Delta t}^{cr} + \frac{\Delta t}{2} \cdot (\underline{V}^{cr})^{-1} \cdot [(\underline{s}_t^{cr})^i + \underline{s}_{t-\Delta t}^{cr}]. \tag{19c}$$

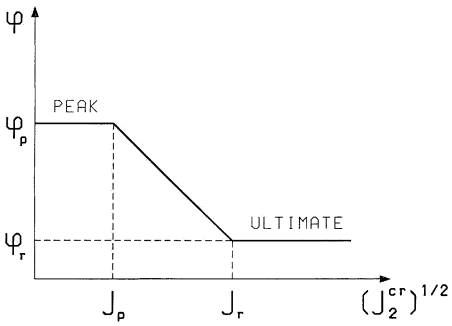


**Fig. 8.** Variation of the friction angle with increasing deviatoric creep strain

4) The unbalanced nodal force vector for the subsequent iteration is computed through the following equation,

$$\underline{r}_t^i = \sum \int_V \underline{B}^T \underline{D} \cdot [(\underline{\varepsilon}_t^{cr})^i - (\underline{\varepsilon}_t^{cr})^{i-1}]\, dv. \tag{20}$$

5) A convergence test is carried out based on the norm of the unbalanced forces. The analysis continues with the next time increment if the test is fulfilled, otherwise a further iteration is performed for the current step.

It has been observed that the so-called "tertiary" creep could play a non negligible role in the overall time dependent behaviour of the rock masse. It involves, in fact, an increase of the rate of deformation, under a constant stress state, which may eventually lead to a global failure of the mass. This behaviour can be introduced in the adopted creep model by providing a suitable law, governing the variation of the visco-plastic parameters with increasing non-reversible strains. To this purpose, the simple relationship graphically depicted in Fig. 8 has been adopted here.

The shear strength ($\alpha$ and $k$) and viscosity ($\eta$) parameters are considered as functions of a scalar measure of the non reversible strains, here represented by the square root of the second invariant $J_2^{cr}$ of the deviatoric creep strains $\underline{e}^{cr}$. Alternately, the cumulated plastic strain work can be adopted.

The material parameters keep their "peak" values until the deviatoric plastic deformation reaches a first limit value $J_p$. Then a linear reduction of the parameters takes place, with increasing plastic strains, which brings them to their "residual" values when the deviatoric deformation reaches a second limit $J_r$.

It seems worthwhile mentioning that the dilatant behaviour of the rock mass should be limited to avoid an excessive volume increase during the development of secondary and tertiary creep. To this purpose, a vanishing residual value for the dilatancy angle (characterising the plastic potential $\Psi$) was adopted in the analyses of the slide, so that no further volume increase takes place when the residual condition is attained.

The iterative procedure previously outlined can still be adopted, even in the presence of tertiary creep, if the material parameters are assumed constant within

each time increment and their values are evaluated on the basis of the average irreversible deformation during the step.

It has to be observed that too large values of the time increment could lead to the instability of the time integration process when a sharp reduction of the material parameter, and in particular of the viscosity, takes place. A simple automatic procedure was implemented into the finite element program to avoid this drawback.

The iterations for each time step initiate using the corresponding time increment provided by the user. The vector of the residual nodal forces, calculated at the end of each iteration, is compared with that obtained at the end of the previous iteration. The instability of the integration process is induced by the increase of the residual forces at some nodes of the mesh. If this condition is detected, the time increment is reduced by a factor provided by the user (say 0.5) and the time step is repeated.

This procedure turns out to be effective, for the cases solved so far, and it does not involve a marked increase of computer time, since the instability condition is usually detected during the first few iterations of the time step.

## 6. Particular Aspects of the Numerical Analysis of the Slope

To set up the finite element model for Rosone slide it was necessary to make a series of choices related to the stress/strain regime and to the sequence of steps adopted in the analyses. First, considering the difficulties related to a three-dimensional discretization of the geological features of the rock mass, and the computational burden involved by the consequent visco-plastic analysis, it was decided to base the calculations on a two-dimensional, plane strain finite model of the slope. Even though this would limit the accuracy of results, it would still permit an insight into the causes leading to the movement of the slide.

As to the phases into which the analysis has to be subdivided, they can be summarised as follows: 1) Determination of the stress state in the rock mass subjected to its own weight and to the action exerted by the glacier. 2) Simulation of the melting process of the glacier. 3) Simulation of the changes of the water table level within the slope.

A first attempt to evaluate the initial stress distribution was based on meshes limited to the upper part of the slope, a simplified scheme which is depicted in Fig. 9. Initially, to test the accuracy of this simple scheme, the evaluation of the stress state was attempted within an unlimited slope having a constant inclination and subjected only to its own weight. Unfortunately this led to a series of problems in defining the boundary conditions on the vertical and bottom sides of the mesh. The details of this part of the study, which are not presented here for briefness, can be found in (Borgonovo and Isoli, 1997).

It turned out that a proper initial state of stress can be derived only if the vertical boundaries (A–B and C–D in Fig. 9) are subjected to a pressure distribution linearly increasing with depth and if the vertical displacements of the nodes of the bottom boundary (B–C) are constrained. However, these constraints cannot be

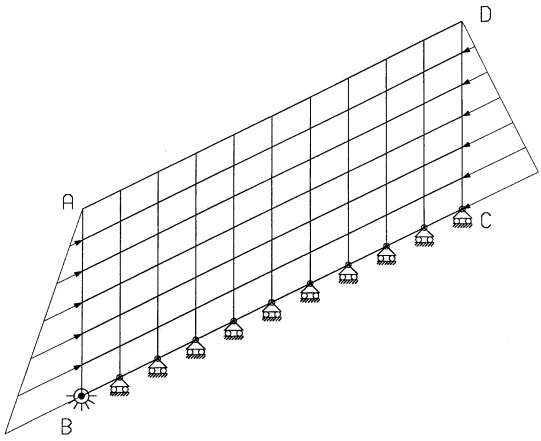


**Fig. 9.** A simplified mesh for the shallow portion of the slope

adopted when the pressure of the glacier (having both vertical and horizontal components) is applied to side A–B of the slope. In fact, the vertically constrained bottom boundary moves horizontally and a high stress concentration develops in the vicinity of the corner B where the horizontal displacement is constrained to avoid singularity of the stiffness matrix.

In other words, it seems that a proper initial stress state could be obtained only by modifying the boundary conditions according to the applied loads. This would be possible, in principle, but it would then lead to an ambiguity in choosing the boundary constraints for the second and third step of the analysis, simulating the melting of the glacier and the changes in the water table level.

To avoid this ambiguity, it was decided to adopt a larger mesh that discretizes also the deep portion of the rock mass (Fig. 10). In this case the horizontal dis-

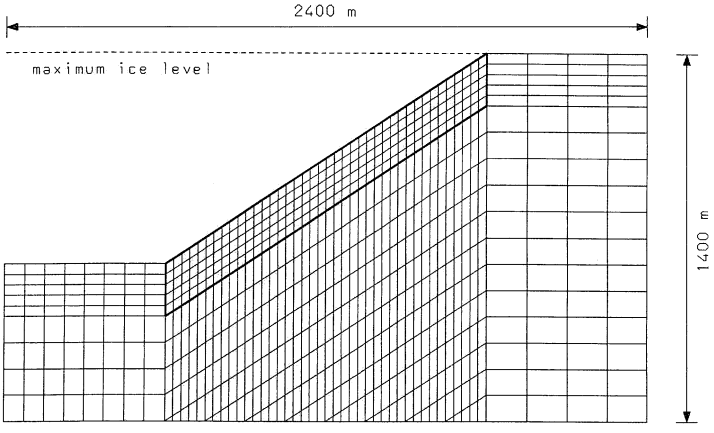


**Fig. 10.** A simplified mesh for the entire slope

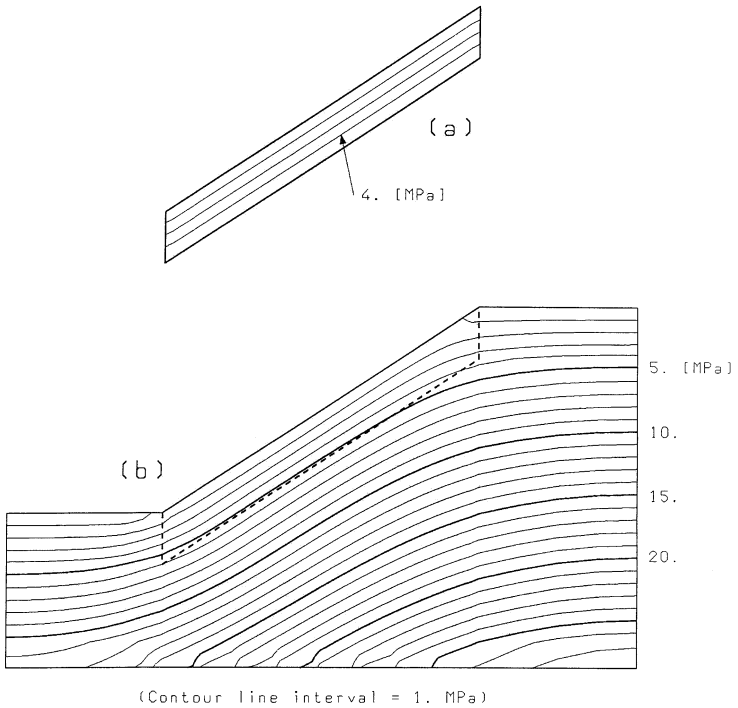


**Fig. 11a,b.** Contour lines of the vertical stress from elastic analyses based on simplified meshes, **a** shallow and **b** complete, subjected to the own weight of the rock

placement was constrained on the two vertical sides of the mesh, while the vertical displacement was set to zero on its bottom boundary. As an example of the mesh influence on the results of calculations, the vertical stress distributions obtained by elastic analyses based on the "shallow" (Fig. 9) and "complete" (Fig. 10) meshes are shown in Figs. 11 and 12, respectively. Note that the two meshes lead to quite similar (and correct) results when subjected to the rock own weight. On the contrary, only the complete mesh is able to provide a reasonable stress distribution when also the pressure exerted by the glacier is applied on the slope surface.

As previously mentioned, the first two phases of the finite element analysis require the evaluation of the stress state within the slope subjected to the rock's own weight and to the action of the glacier and, subsequently, the simulation of the melting process of the glacier.

Two alternative procedures have been considered for introducing the action of the glacier in the calculations. The first one consists in discretizing only the rock mass and in subjecting the slope surface to a normal pressure distribution corresponding to the action of the glacier. This distribution is then modified in steps to simulate the reduction of the glacier height during time, due to its melting. An alternative approach consists in dicretizing into finite elements both slope and glacier, and then removing by layers the part of the mesh corresponding to the glacier.

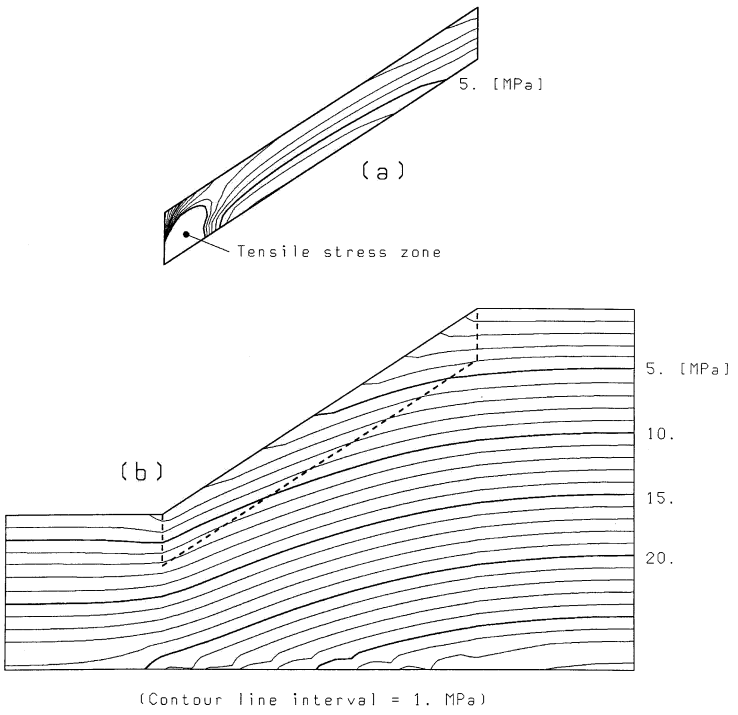


**Fig. 12a,b.** Contour lines of the vertical stress from elastic analyses based on simplified meshes, **a** shallow and **b** complete, subjected to the own weight of the rock and to the pressure of the glacier

Both approaches were adopted in some test examples. In the first case the mesh of Fig. 10 was directly adopted in the calculations. A rectangular mesh was used in the second case, the part of which that represents the rock mass coincides with the mesh in Fig. 10. A dashed line in Fig. 10 represents the ice level at the beginning of calculations.

The results of elastic and elasto-plastic analyses based on the two meshes, assuming a homogeneous rock mass, showed that the results of the two approaches are practically equivalent. Since the first one is more convenient in terms of mesh generation and data handling, it was decided to use this procedure for the subsequent analyses of the slope.

The third phase of the analysis should account for the changes of the water table level within the slope, introducing the "driving" effect caused by the pore pressure distribution.

To this purpose, a seepage analysis is first performed, adopting the same mesh used for the stress analyses, which leads to the hydraulic head distribution within the slope.

Then, the nodal hydraulic head vector $\underline{h}$ is converted into "equivalent" (in the finite element sense) seepage nodal forces $\underline{f}_w$ (see e.g. Cividini et al., 1986; 1996) through the following equation,

$$\underline{f}_w = \underline{C} \cdot \underline{h}, \tag{21}$$

where $\underline{C}$ is the so-called "coupling" matrix,

$$\underline{C} = \sum \int_V \underline{B}^T \cdot \underline{m} \cdot \underline{b}_w^T \, dv. \tag{22}$$

In Eq. (22) the summation runs over the elements of the mesh, $V$ represents the element volume, $\underline{B}$ is the matrix collecting the spatial derivatives of the shape functions used to describe the displacement field within the elements, $\underline{b}_w$ is the column vector of the shape functions of the hydraulic head and $\underline{m}$ is defined by Eq. (3).

The nodal force vector $\underline{f}_w$ is then introduced in the visco-plastic analysis of the slope as an additional contribution to the external loads.

A further problem that showed up concerns the value of the viscosity parameter. In fact, while the elastic and shear strength constants can be worked out on the basis of the available experimental data, no direct information is available on the viscosity of the creep model.

The evaluation of the order of magnitude of this parameter was based on a simple test problem in which the slope was modelled by two superimposed visco-plastic blocks sliding on an inclined plane. The blocks were subjected to the rock's own weight and to the pore pressure measured by piezometer A1 at depths of 29 m and 41 m, and shown in Fig. 6.

A back analysis (see e.g. Sakurai and Takeuchi) was then carried out to evaluate the order of magnitude of the viscosity coefficient. In general terms a back analysis consists in finding the values of the mechanical parameters characterising the rock mass that, when introduced in the stress analysis of the problem under examination, lead to results as close as possible to the corresponding in situ measurements.

Note that in the present context only one free parameter exists, i.e. the coefficient of viscosity, and that the in situ measurements are represented by the horizontal displacements of the slope recorded by the inclinometers.

Various techniques have been proposed in the field of soil/rock engineering for solving back analysis problems (see e.g. Gioda and Sakurai, 1987). They are in general based on the minimisation of an error function, representing the discrepancy between the field measurements and the corresponding quantities evaluated through a numerical model of the problem at hand.

In most cases the error is a complicated non-linear function of the unknown parameters, and it is not possible to work out the analytical expression of its gradient. This is particularly the case for visco-plastic problems. Therefore, the adopted minimisation algorithm must handle general non-linear functions and it should not require the analytical evaluation of their gradient.

Methods of this kind, known in mathematical programming as Direct Search Methods (Himmelblau, 1972), are iterative techniques that perform the minimisation process by comparing the values of the error function during a sequence of successive evaluations of it.

For the problem at hand, each evaluation requires the solution of the two-block problem on the basis of the trial value of the coefficient of viscosity chosen by the minimisation algorithm for that iteration.

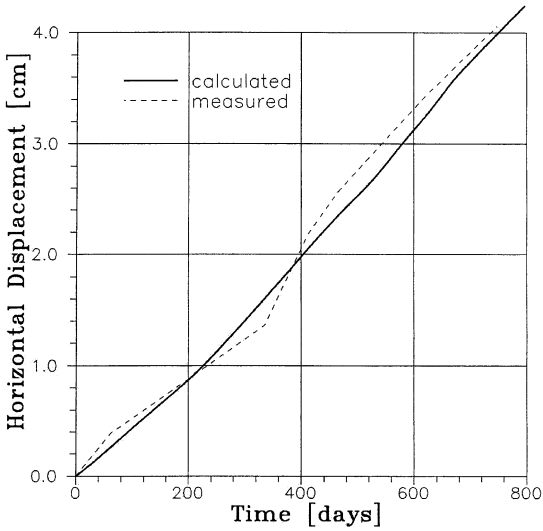


**Fig. 13.** Comparison between the measured movement of the slope and the displacement obtained by the "two-block" scheme

Here the minimisation process has been based on Rosenbrock algorithm and on the following definition of the error function $E_r$,

$$E_r = \sum_{i=1,n} [u_i^* - u_i(\underline{p})]^2. \tag{23}$$

In Eq. (23), $u_i^*$ represents the n displacements measured in the field and $u_i$ are the corresponding numerical results, which depend on the unknown parameters collected in vector $\underline{p}$.

In most practical cases some limiting values exist for the entries of vector $\underline{p}$. For instance, the viscosity coefficient should be greater than zero. These limits, expressed by inequality constraints, can be easily taken into account in the minimisation process. In fact, if one of them is violated, a very high value is assigned to the error function so that the minimisation algorithm automatically drives back the optimisation path into the feasible region.

The back analysis procedure led to an order of magnitude of the viscosity coefficient between 10 and 100 Pa · s. A comparison between calculated and measured horizontal displacements at the slope surface is shown in Fig. 13 for the "optimal values" of the material parameters. Due to the exceedingly simple scheme adopted, the mentioned range of viscosity merely represents an initial suggestion to be subsequently refined through a more detailed numerical model.

## 7. Finite Element Model and Results of Calculations

Having reached some insight into the relevant characteristics of the finite element model for Rosone slide, in terms of stress-strain regime, boundary conditions and

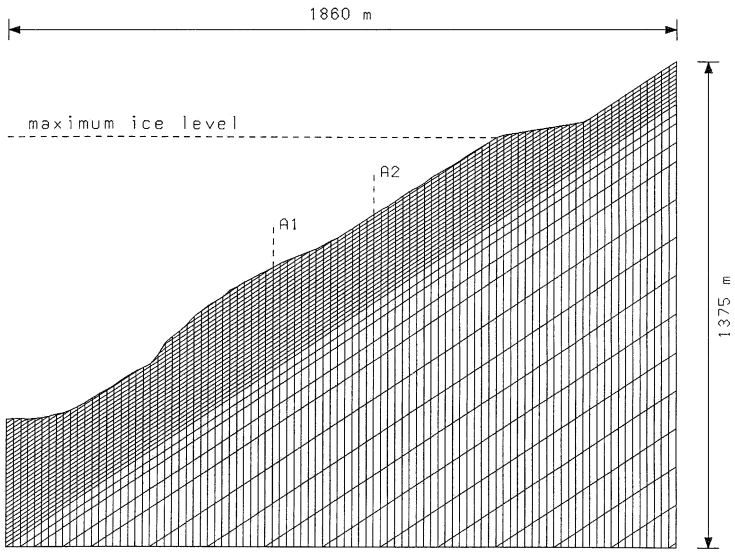


**Fig. 14.** Finite element mesh for Rosone slide

material properties, the mesh depicted in Fig. 14 was developed for the entire slope. The mesh is based on the present shape of the slope with reference to the section shown in Fig. 5. This introduces an obvious limitation in the results of calculations, since the evolution of its geometry during time is not taken into account. It should be recognised, however, that such a limit could not be easily eliminated due to the lack of the necessary geological information. Note that, to reduce the influence of discretization, it was attempted to keep a constant size of the elements in the upper part of the slope where most of the time dependent deformation takes place.

Figure 14 reports also the maximum ice level (dashed line) assumed in the calculation, about 800 m above the valley bottom.

The mesh, consisting of 2803 nodes and of 2705 four node, isoparametric elements, is subdivided into 4 regions (referred to as zones I to IV in Fig. 15), having different material properties. Figure 15 shows also the three levels of the water table (low, medium and high) considered in the calculations.

Note that the analyses discussed in the following do not aim at simulating the long-term time dependent behaviour of the slide during its entire geological "history". They merely intend to provide some insight into the short-term effects caused, in particular, by the fluctuation of the water table.

As previously mentioned, it is first necessary to evaluate the stress state within the slope at the end of the melting of the glacier. This is the "reference" conditions for the visco-plastic analysis, where the water table variation is accounted for.

The evaluation of this reference state requires three subsequent analyses. The first one evaluates the stress state in the slope subjected to the rock's own weight and to the pressure exerted by the glacier. Then this pressure is reduced in steps,

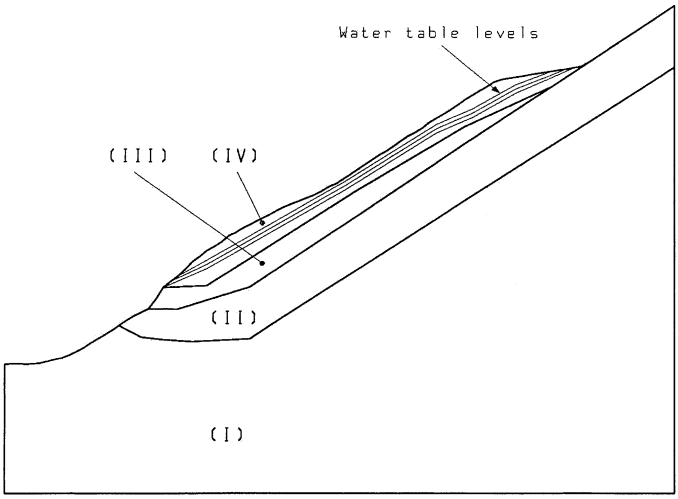


**Fig. 15.** Zones with different mechanical characteristics and levels of the water table

simulating the melting of the glacier. Finally, the nodal forces equivalent to the pore pressure for the "low" water table level are applied to the mesh, following the procedure described in the previous Section.

This first stage of calculations was carried out, assuming an elasto-plastic behaviour for entire the rock mass. In fact, the lack of quantitative information on the movements of the slope during its geological evolution did not permit an estimation of the overall viscosity parameters for such a long time span.

Various analyses were performed to work out an initial stress state that did not lead to a collapse condition for the entire slope and to "tune" the values of the shear strength constants. They were based on different sets of the strength parameters, within the range suggested by the available geological/geotechnical data.

As a result, the slope was subdivided into the four mentioned zones (cf. Fig. 15). Zone (I) has a linear elastic behaviour. Zone (II) is elastic-perfectly plastic, with cohesion $c = 10000$ KPa and friction angle $\varphi = 40°$. Zones (III) and (IV) are characterised by softening effects with the following values of the peak and residual cohesion and friction angle:

$$\text{Zone(III)}: c_p = 3500 \text{ KPa}, \quad \varphi_p = 40°; \quad c_r = 1500 \text{ KPa}, \quad \varphi_r = 38°$$

$$\text{Zone(IV)}: c_p = 800 \text{ KPa}, \quad \varphi_p = 38°; \quad c_r = 35 \text{ KPa}, \quad \varphi_r = 32°$$

To account for the influence of joints and faults, the elastic parameters of the rock mass were evaluated by properly scaling down those of the rock material recovered from the borings.

It has been observed that the visco-plastic material model allows for the reduction of the shear strength parameters with increasing deviatoric plastic strains, depending on the values assumed for $J_p$ and $J_r$ (cf. Fig. 8). Considering the brittle

behaviour of rocks, a very small value of $J_r > J_p$ has been adopted in the calculations. This implies that the rock mass behaves elastically until the peak yield limit is reached. Then, a rapid reduction of the shear strength parameters takes place, leading to the residual yield condition.

The stress state derived by this elasto-plastic calculation was adopted as the initial condition of a series of visco-plastic calculations where the effects of the changes in the water table level were simulated. Note that the initial stress distribution is completely "carried out" by the frictional component of the constitutive model (cf. Fig. 7). Hence, no time dependent deformation is associated to it.

The visco-plastic analyses were based on the previously defined shear strength parameters, while different values of the viscosity parameters of zones (III) and (IV) were adopted starting from the values defined by the previously mentioned two-block scheme.

The results of these calculations were compared to the readings of the inclinometers placed at locations A1 and A2 in Fig. 14, for a time span of 200 days. An acceptable agreement between numerical and experimental data was obtained when the viscosity coefficients for zones (III) and (IV) were equal to 15 Pa · s and to 4 Pa · s, respectively.

A summary of the numerical results is shown in Figs. 16 and 17. The first one presents the contour lines of the second invariant of the deviatoric plastic strains for medium and high water table levels. No appreciable time dependent movements were evaluated in the first case, and a minor increase of the plastic deformation was observed (cf. Fig. 16a) with respect to that corresponding to the initial state.

On the contrary, the slope deformation increased with time when the water table was brought to its high level, as shown by Fig. 16b that presents the contour lines of the non-reversible deviatoric strains at 200 days.

The comparison between the inclinometer data at 200 days and the numerical results at 50, 100, 150 and 200 days is presented in Fig. 17. These data indicate that the change in the water table level is likely to be one of the causes of the observed movements of the slope. They also show that the assumption of a constant value of viscosity within the slope zones leads to an acceptable estimation of the slope movement, but does not permit a detailed interpretation of the locally measured displacements.

## 8. Concluding Remarks

A numerical analysis, based on a finite element method, has been discussed with reference to the movements of the deep gravitational slide of Rosone, located in the Piemonte region in northern Italy. The results of this study suggest some conclusions on the problems encountered in the finite element modelling of this kind of phenomena and some insight into the specific aspects of the examined slide.

In general terms, it could be observed that a finite element discretization, limited only to the upper portion of the rock mass, does not permit a consistent evaluation of the stress distribution for the various loading conditions that char-

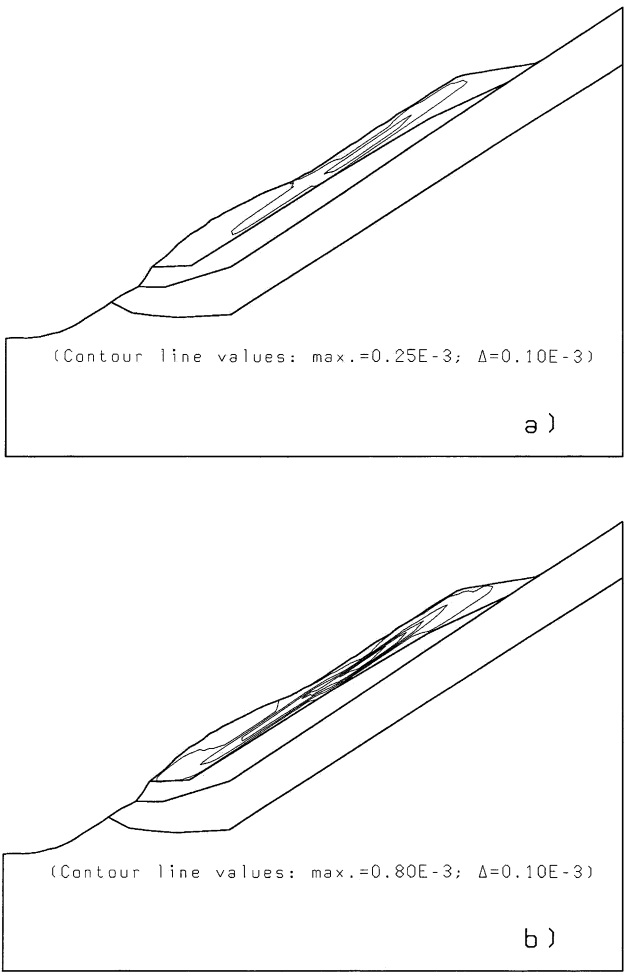


**Fig. 16a,b.** Contour lines of the deviatoric plastic strains: **a** medium and **b** high levels of the water table

acterise the geological history of the slope. It was also noted that a proper examination of the time dependent downward movements requires the use of a proper visco-plastic creep model, accounting for the development of strain softening effects, i.e. of the reduction of the overall shear strength of the rock mass with increasing non-reversible deformation.

The detailed simulation of the geological history of the slide would require an adequate evaluation its "initial" stress/strain state and of the changes in its geometry. This, however, is a difficult task due to the lack of consistent geological information for such a long time span. Also the quantitative definition of the overall strain softening effects seems an ambitious goal, since the available experimental information is too limited to properly define the behaviour of the wide rock mass involved by the slide.

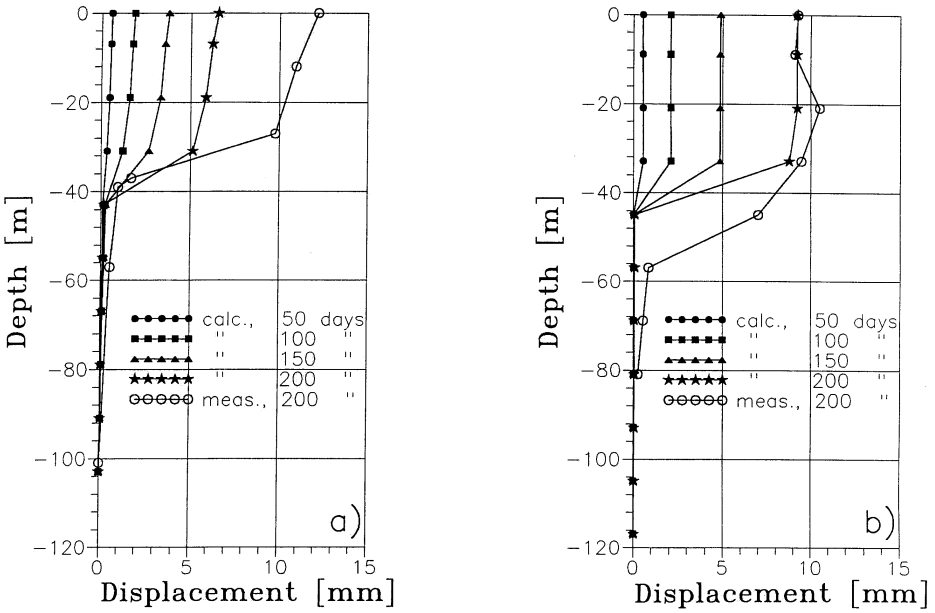


**Fig. 17.** Comparison between calculated displacements and those derived from the measurements of inclinometer A1 **a** and A2 **b**

In this respect, the so-called back analysis of in situ measurements could provide a sound base for calculations. However, technical and economical constraints represent a limit to the in situ investigation that is often difficult to overcome.

As to the specific problem of Rosone slide, the results of analyses show that the change of the water table level during time is probably a main cause of the observed movements.

The numerical model adopted in this study assumes a constant value of the mechanical parameters within the zones in which the slide was subdivided. This, however, appears as a drawback for a detailed interpretation of the in situ measurements. Also this limit could have been overcome if additional experimental data had been available.

Concluding, it seems that the difficulties in defining the initial stress/strain distribution within the rock mass, and the limited geological and geotechnical information, represent substantial drawbacks for the numerical interpretation of this kind of long term, time dependent movement. These limits could be, at least partially, removed if more detailed data were available, mainly from in situ investigations carried out during a sufficiently long time span.

## Acknowledgements

The financial support of the Ministry of University and Research of the Italian Government is gratefully acknowledged. The Authors wish to thank A. Cividini, for her contribution concerning the theoretical aspects of the finite element approach, D. Sterpi, B. Borgonovo

and A. Isoli, for their valuable help in performing the numerical analyses, and S. Campus for his effort in organising the geological data.

## References

Barla, G., Chiriotti, E. (1995): Insights into the behaviour of the large deep-seated gravitational slope deformation of Rosone, in the Piemonte region (Italy). Proc., 44th Geomechanics Colloquium, Salzburg, 425–432.

Borgonovo, G., Isoli, A. (1997): Modellazione ad elementi finiti della deformazione gravitativa profonda di un versante. Laurea thesis, Department of Structural Engineering, Politecnico di Milano, Milan, Italy.

Chiriotti, E. (1997): Mathematical modelling of the behaviour of the large deep-seated gravitational slope deformation of Rosone (in italian). PhD thesis, Politecnico di Torino, Turin, Italy.

Cividini, A., Gioda, G., Barla, G. (1986): A numerical analysis of tunnels in saturated two-phase media, Proc., 11th Int. Conf. on Soil Mechanics and Foundation Engineering, San Francisco.

Cividini, A., Garigali, G., Manassero, V. (1996): A numerical interpretation of the observed behaviour of an unstable slope. Proc., ISRM Symp. on Prediction and Performance in Rock Mechanics and Rock Engineering, Torino.

Cristescu, N. (1988): Rock rheology. Kluwer Academic Publishers, Dordrecht.

Cristescu, N., Gioda, G. (eds.) (1994): Visco-plastic behaviour of geomaterials, CISM Courses and Lectures No. 350, Springer, Wien New York.

Forlati, F., Mortara, G. (1994): Deep deformations in Western Alps (Piemonte and Valle d'Aosta), in deep-seated gravitational slope deformations and large-scale landslides in Italy. Special volume IAEG International Congress, Lisbon, 11–14.

Forlati, F., Ramasco, M., Susella, G. F., Barla, G., Marino, M., Mortara, G. (1991): La deformazione gravitativa di Rosone. Un approccio conoscitivo per la definizione di una metodologia di studio, Proc., Conf. on ''Fenomeni franosi. Interventi di salvaguardia del territorio e proposte per la pianificazione urbanistica''. Acta Geologica 68, 71–108.

Forlati, F., Brovero, M., Campus, S. (1995): Alcune considerazioni sulle deformazioni gravitative profonde di versante inerenti il territorio piemontese. Proc., 2nd International Meeting for Young Researchers in Applied Geology, Peveragno, Cuneo, Italy.

Fritz, P. (1984): An analytical solution for axisymmetric tunnel problems in elasto-visco-plastic media. Int. J. Numer. Anal. Meth. Geomech. 8, 325–342.

Ghaboussi, J., Gioda, G. (1977): On the time dependent effects in advancing tunnels. Int. J. Numer. Anal. Meth. Geomech. 1, 249–269.

Gioda, G. (1981): A finite element solution of non-linear creep problems in rocks. Int. J. Rock Mech. Min. Sci. 18, 34–46.

Gioda, G., Sakurai, S. (1987): Back analysis procedures for the interpretation of field measurements in geomechanics. Int. J. Numer. Anal. Meth. Geomech. 11, 555–583.

Himmelblau, D. M. (1972): Applied non-linear programming. McGraw-Hill, New York.

Kovari, K., Fritz, P. (1983): Rheo-Staub users' manual. ETH, Federal Institute of Technology, Zurich.

Ladanyi, B. (1993): Time-dependent response of rock around tunnels. In: Hudson, J. A. et al. (eds.), Comprehensive rock engineering. Pergamon Press, Oxford.

Mortara G., Sorzana P. F. (1984): Slope instability in high mountain environments: deep-seated gravitational deformations in Western Alps (Italy), CNR-PAN Meeting on progress mass movement and sediment transport study, Turin, 77–84.

Ramasco, M., Stoppa, T., Susella, G. F. (1989): La deformatione gravitativa profonda di Rosone in Valle dell'Orco. Bull. Italian Geological Society 108, 401–408.

Sakurai, S., Takeuchi, K. (1983): Back analysis of measured displacements of tunnels. Rock Mech. Rock Engng. 16, 173–180.

Vulliet, L. (1995): Predicting large displacements of landslides. Proc., 5th Int. Conf. on Numerical Models in Geomechanics, Davos, Switzerland, 527–532.

Vulliet, L. (2000): Natural slopes in slow movement. In: Zaman, M. et al. (eds.), Modelling in geomechanics. J. Wiley&Sons, Chichester, 653–676.

Zienkiewicz, O. C., Cormeau, I. C. (1974): Viscoplasticity, plasticity and creep in elastic solids. Int. J. Numer. Meth. Engng. 8, 821–845.

Zienkiewicz, O. C., Pande, G. N. (1977): Time dependent multilaminate model for rocks – A numerical study of deformation and failure of rock masses. Int. J. Numer. Anal. Meth. Geomech. 11, 219–247.

**Authors' address:** Prof. Giancarlo Gioda, Politecnico di Milano, Dipartimento di Ingegneria Strutturale, Piazza Leonardo da Vinci 32, I-20133 Milano, Italy.
E-mail: gioda@stru.polimi.it